Structural study of amorphous zinc-ferrite film by the anomalous X-ray scattering method



1992 J. Phys.: Condens. Matter 4 6355

(http://iopscience.iop.org/0953-8984/4/30/002)

J. Phys.: Condens. Matter 4 (1992) 6355–6366. Printed in the UK

# Structural study of amorphous zinc-ferrite film by the anomalous x-ray scattering method

Y Waseda†, E Matsubara†, K Okuda†§, K Omote†||, K Tohji†¶, S N Okuno‡ and K Inomata‡

† Research Institute of Mineral Dressing and Metallurgy (SENKEN), Tohoku University, Aoba-ku, Sendai 980, Japan

‡ Research and Development Centre, Toshiba Corporation, Komukai Toshiba-cho, Saiwai-ku, Kawasaki 210, Japan

Received 31 January 1992, in final form 13 April 1992

**Abstract.** The anomalous x-ray scattering (AXS) method using Zn and Fe K-absorption edges has been applied to a structural study of amorphous zinc-ferrite film (1.4 $\mu$m in thickness) grown on a silicate glass substrate. The possible atomic arrangements in near-neighbour regions of amorphous zinc-ferrite films were estimated by reproducing the differential intensity profiles for Zn and Fe as well as the ordinary diffraction profile using the least-squares technique for the interference function. It is then suggested that Zn and Fe atoms are likely to occupy both tetrahedral and octahedral sites formed by oxygens. This result has also been confirmed by the EXAFS analysis using the in-house EXAFS facility.

## 1. Introduction

Various amorphous oxides have been produced by several methods such as rapid quenching from the melt and ion-beam sputtering, and some of these new oxide systems appear to indicate the technological potential for advanced magnetic materials. On the other hand, both physical and chemical properties of thin films are applied to many new functional materials, such as magnetic or optical memory devices; this includes amorphous oxide films grown on a substrate.

The amorphous ferrite films prepared by ion-beam sputter deposition have received much attention recently because of their spin glass behaviour [1]. This is, of course, related to the novelty of their physics, arising mainly from the peculiar non-periodicity of their atomic arrangements. Thus, knowledge of the near-neighbour atomic correlations of cations in these ferrite films is essential to an understanding of the interesting magnetic properties at a microscopic level.

In the quantitative structural analysis of a thin film grown on a substrate, the scattering intensity from the substrate should be eliminated accurately from the total scattering intensity of a sample. However, this is known to be a complicated task due

§ Present address: Kawasaki Steel Corp., Technical Research Division, Kawasaki-cho, Chiba 260, Japan.

|| Permanent address: Kimura Metamelt Project, ERATO, Research Development Corporation of Japan.

¶ Department of Resources Engineering, Faculty of Engineering, Tohoku University, Aoba-ku, Sendai 980, Japan.

0953-8984/92/306355+12$04.50  

to difficulties arising in the subtraction process in estimating the scattering intensity of the film alone. With respect to this point, the use of the anomalous x-ray scattering (AXS) method has recently been found to result in a significant breakthrough as it reduces the difficulty in the subtraction process [2].

In the present study, by applying the AXS method to an amorphous zinc-ferrite film (1.4 $\mu$m in thickness) grown on a silicate glass substrate, we will obtain structural information, including atomic arrangements in the near-neighbour region.

## 2. Principle of the structural analysis using the AXS method

The reflection mode of the Seemann–Bohlin geometry with a small incident angle, $\alpha$, of the order of 1°, is widely used for structural analysis of thin films [3], so as to satisfy the condition that the penetration depth of the beam becomes small and scattering from the sample surface large relative to scattering from the bulk. Since the measured intensity consists of the intensities from a film and the substrate supporting it, the contribution from the substrate should be eliminated to obtain the intensity attributable to the film alone. This subtraction process is known to be one of the main sources of experimental error in the structural analysis of thin films. The relatively new procedure using the AXS method does not include this subtraction process nor the conventional normalization procedure, such as the Krogh-Moe-Norman method (for example, see [4]) required for converting the measured intensity data into absolute units. For convenience, the fundamentals of the procedure using the AXS method [2] are given below.

When the intensity of the incident beam is monitored by an ion chamber located just in front of the sample during the course of measurement, it is related to the power of the incident beam for a certain period of time ($tP_0$) as follows.

$$tP_0 = (E_p I_m / EeG_a G_v)\exp(-\mu_a l_1)\exp[-\mu_i(l_t + l_e)/2]/(1 - \exp(-\mu_i l_e)) \quad (1)$$

where $I_m$ is the total monitor count for a certain counting time $t$, $E_p$ is the energy to form an ion–electron pair, $\mu_i$ and $\mu_a$ are the linear absorption coefficients of gas used for the ion chamber and air, $l_t$, $l_e$ and $l_1$ are the total length of the ion chamber, the length of the electrode in the ion chamber and the distance from the ion chamber to the sample, respectively. $E$ is the energy of incident photons, $e$ is the electron charge, $G_a$ and $G_v$ are the gain of the current amplifier and the conversion gain of the voltage–frequency converter. The measured intensity $I_{obs}$ is given by the following formula using (1) for $tP_0$.

$$I_{obs}(Q, E) = CP[(\rho_f A_f / M_f) I_{eu,f}(Q, E) + (\rho_s A_s / M_s) I_{eu,s}(Q, E)] \quad (2)$$

where

$$A_f = [\sin(2\theta - \alpha)/2\mu_f \sin\theta\cos(\theta - \alpha)] \times [1 - \exp(-2\mu_f t_f \sin\theta\cos(\theta - \alpha)/\sin\alpha\sin(2\theta - \alpha))] \quad (3)$$

$$A_s = [\sin(2\theta - \alpha)/2\mu_s \sin\theta\cos(\theta - \alpha)] \times \exp[-2\mu_f t_f \sin\theta\cos(\theta - \alpha)/\sin\alpha\sin(2\theta - \alpha)] \quad (4)$$

$$C = tP_0(e^4/m^2c^4)(wh/r^2)N_A. \quad (5)$$

The quantity $2\theta$ is the angle between the incident and diffracted beams, $\mu_f$ and $\mu_s$ are the linear absorption coefficients of the film and substrate, respectively; $P$ is the polarization term (almost equal to 1 for the synchrotron radiation in the present study), $N_A$ is Avogadro's number, $m$ is the electron rest mass and $c$ is the velocity of light. $w$ and $h$ are the width and height of the diffracted beam on the counter and $r$ is the distance from the sample to the counter. The values of $\rho_f$ and $M_f$ are the density and the atomic weight of the film, and $\rho_s$ and $M_s$ are similarly defined for the substrate. $I_{eu,f}$ and $I_{eu,s}$ are the scattering intensities from the film and substrate in absolute units, respectively.

When the anomalous x-ray scattering occurs with respect to an element of A, the total x-ray atomic scattering factor $f$ becomes complex and can be expressed by

$$f_A(Q,E) = f_A^0(Q) + f_A'(E) + i f_A''(E) \tag{6}$$

where $f^0$ corresponds to the usual atomic scattering factor of A at an energy sufficiently far from the absorption edge, and $f'$ and $f''$ are the real and imaginary parts of the anomalous dispersion terms of A. For example, the anomalous dispersion terms of Zn, Fe and O in an energy range including Fe and Zn K-absorption edges, which are theoretically calculated [5] with Cromer and Liberman's scheme [6], are shown in figure 1. In this figure, the incident energies used for the present AXS measurements at each edge are labelled A to D. It may be worth mentioning that the values of $f'_{Fe}$ at A and B or $f'_{Zn}$ at C and D in figure 1, for example, show a drastic change at the lower energy side of their own absorption edge, whereas those of $f''_{Fe}$ or $f''_{Zn}$ are almost constant in this energy region. Such salient features are true in all elements except for the energy region of the respective absorption edge [7].

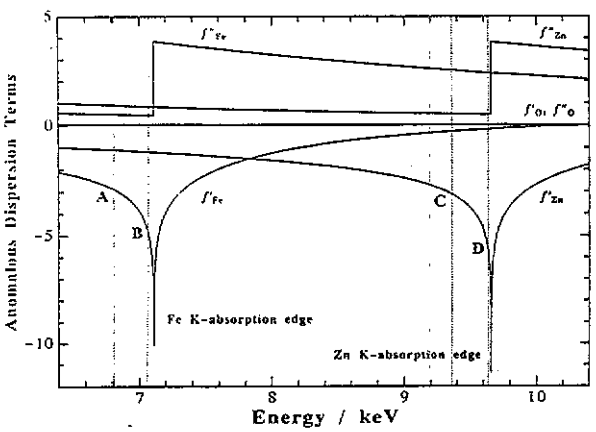


**Figure 1.** Theoretical energy dependence of anomalous dispersion terms for Zn, Fe and O near the Zn and Fe K-absorption edges, as calculated using Cromer and Liberman's method [6]. The incident energies used in the present AXS measurements at the Fe and Zn K-absorption edges are labelled A to D.

Here, consider that the energy of the incident beam is tuned to within the vicinity of the absorption edge of the constituent element A in the film. In this energy region, the atomic scattering factors of constituents other than the A element, including the substrate, are almost unchanged because their anomalous dispersion terms are almost constant. Furthermore, at the lower energy side of the edge, the linear absorption

coefficients of all the elements including element A are theoretically evaluated and give almost constant values. Consequently, the following simplification can be made, as was shown in previous work [2].

The difference of the scattering intensities in absolute units measured at the two energies $E_1$ and $E_2$ below the absorption edge can be reduced to the following equation, using (2):

$$\Delta I_{eu}(Q, E_1, E_2) = I_{eu,f}(Q, E_1) - I_{eu,f}(Q, E_2)$$
$$= (M_f/CPA_f\rho_f)[I_{obs}(Q, E_1) - I_{obs}(Q, E_2)]. \tag{7}$$

By subtracting the difference of the mean square of the atomic scattering factors $\langle f^2 \rangle$ at these two energies from the intensity difference in (7), the intensity function of $\Delta i_A$ becomes

$$\Delta i_A(Q, E_1, E_2) = \frac{\Delta I_{eu}(Q, E_1, E_2) - (\langle f^2(Q, E_1)\rangle - \langle f^2(Q, E_2)\rangle)}{W(Q, E_1, E_2)}$$
$$= \frac{x_A(f'_A(E_1) - f'_A(E_2))}{W(Q, E_1, E_2)} \int_0^\infty 4\pi r^2 \sum_{j=1}^{N}$$
$$\times \Re[f_j(Q, E_1) + f_j(Q, E_2)](\rho_{Aj}(r) - \rho_{0j}) \frac{\sin(Qr)}{Qr} \, dr \tag{8}$$

$$W(Q, E_1, E_2) = \sum_{j=1}^{N} x_j \Re[f_j(Q, E_1) + f_j(Q, E_2)] \tag{9}$$

where $x_j$ is the atomic fraction of the element $j$, and $N$ the total number of constituent elements in the film. $\Re$ denotes the real part of the values in the brackets. Equation (8) suggests that the intensity function of $\Delta i_A$ enables us to obtain structural information about the film alone, because the contribution from the substrate including the Compton scattering is automatically eliminated by taking the difference at two energies. The Fourier transformation of (8) corresponds to the environmental radial distribution function (RDF) around the element A in the film.

$$4\pi r^2\rho_0 + \frac{2r}{\pi x_A(f'_A(E_1) - f'_A(E_2))} \int_0^\infty Q\Delta i_A(Q, E_1, E_2) \sin Qr \, dQ$$
$$= 4\pi r^2 \sum_{j=1}^{N} \frac{\Re[f_j(Q, E_1) + f_j(Q, E_2)]}{W(Q)} \rho_{Aj}(r). \tag{10}$$

Consequently, it is readily understood that the environmental RDF around element A can be obtained without difficulty in the subtraction process when the AXS method is applied to the thin film analysis [2].

The EXAFS analysis has been widely used for structural studies of various substances and its procedure is now very common (see, for example, [8]). Thus, only essential points employed in this work are given below. The oscillatory part of the x-ray absorption rate for a particular element beyond its absorption edge may be given by the following expression.

$$\chi(k) = \frac{m}{4\pi h^2 k} \sum_j \frac{N_j}{r_j^2} t_j(k) \exp(-2r_j/\lambda_e) \sin(2kr_j + \delta_j(k)) \exp(-2k^2\sigma_j^2) \tag{11}$$

where $h$ is Planck's constant, $k$ the wavevector of a photoelectron, $\lambda_e$ the mean free path of the photoelectrons and $r_j$ and $N_j$ are the radial distance and coordination number of the $j$-type atoms from an absorbing atom, respectively. $t_j(k)$ denotes the backscattering matrix element encountered by photoelectrons, $\delta_j$ the phase shift required to account for the potentials arising from both a central absorbing atom and a neighbouring atom (backscattering), and $\sigma_j^2$ a Debye–Waller-type factor corresponding to the root-mean square positional fluctuations of the central and backscattering atoms. By applying the Fourier transformation, the EXAFS RDF becomes

$$\phi_n(r) = \frac{1}{\sqrt{2\pi}} \int_0^\infty k^n \chi(k) \exp(-2ikr) W(k)\, dk \tag{12}$$

where $W(k)$ is a window function. Referring to the EXAFS results for various substances, $n = 3$ was employed in this work. This RDF provides information about the distribution function of neighbouring atoms for a central absorbing atom. In spite of many impressive advantages of the EXAFS analysis, definite structural information for a non-crystalline system cannot be reduced by the simple Fourier transformation of the EXAFS signal alone because of some restrictions arising from the backscattering amplitude, the phase shift and the mean free path of photoelectrons [9]. Thus, the data processing method usually employed for a non-crystalline system is to obtain a best fit between experimental and calculated EXAFS functions on a trial and error basis.

## 3. Sample preparation and experimental procedure

An amorphous film was prepared by ion-beam sputtering of a target of a sintered body of polycrystalline $ZnFe_2O_{4-x}$. The sputtering was carried out with a beam of argon ions accelerated to 1 keV in an oxygen-gas flow of $6.67 \times 10^{-3}$ Pa. More details of the sample preparation have been given elsewhere [1]. The film of 1.4 $\mu$m in thickness was grown on a silicate glass substrate.

The AXS measurements were carried out at a beam line (6B station) with synchrotron radiation in the Photon Factory of the National Laboratory for High-Energy Physics, Tsukuba, Japan. Details of the experimental set-up and analysis are explained in another publication [10]. Only some necessary additional details are given below.

A monochromatic incident beam at energies from 4 to 21 keV was obtained with an Si(111) double-crystal monochromator. Its optimum energy resolution is about 7 eV at 10 keV. The sample was mounted on a double-axis goniometer placed vertically to eliminate the polarization effect. The incident beam was monitored by a nitrogen-gas-flow-type ion chamber placed in front of the sample. The scattering intensity was measured at each angle for certain preset counts of this ion chamber so as to keep constant the total number of photons incident on the sample. The scattering intensities were measured by a portable-type pure germanium solid state detector. The effect of the higher harmonics diffracted by the Si(333) plane was significant in the present measurements. Therefore, by intentionally detuning the second Si crystal of the double-crystal monochromator with a piezo electric device attached to it, the intensity of the higher harmonics was reduced to less than 0.5% although about one fifth of the intensity of the first-order diffraction was lost. At each angle at least 30 000 counts were collected and about 60 000 counts on average were collected at every scattering angle.

The ordinary x-ray scattering measurement was made by Mo Kα-radiation produced by the rotating-anode-type x-ray generator (RIGAKU RU-200) in operation at 50 kV and 150 mA. A monochromatic parallel beam was obtained with a Ge(111) flat single-crystal monochromator in the incident beam. In this way, the angle of incidence of 1° is accurately set and the beam size on the sample surface is easily adjusted by simply changing the slit size built at the exit of the monochromator housing. The soller slit is also placed to limit the horizontal divergence of 0.57°. After the corrections for absorption and polarization, the measured intensity was converted to electron units per atom with the generalized Krogh–Moe–Norman method using the x-ray atomic scattering factors, including their anomalous dispersion terms [11]. The Compton scattering was corrected using the values reported in [12] and the so-called Breit–Dirac recoil factor.

The EXAFS measurements were performed for Zn and Fe K-absorption edges with the in-house facility using an Si(220) Johansson-cut monochromator ($R = 320$ mm) and the white radiation from a molybdenum target produced by a rotating-anode-type x-ray generator (RIGAKU RU-300) operating at 20 kV and 40 mA for the Zn EXAFS and at 20 kV and 100 mA for the Fe EXAFS. The glass substrate holding the film is very thick so the transmission geometry for the EXAFS measurement is not applicable in the present work and thus the fluorescence technique was used. The intensity of the incident beam was monitored by measuring the Fe K fluorescent radiation from an Fe mesh placed in front of the sample in the EXAFS measurement at the Zn K-absorption edge. Instead of the Fe fluorescence, the Cr K fluorescent radiation from Cr powder was used in the measurement at the Fe K-absorption edge. These fluorescent radiations for monitoring the incident beam and the EXAFS signal from the film were detected by scintillation counters with pulse height analysers. Details of the present EXAFS measurements using the fluorescent radiation in the in-house facility and its further application will be given elsewhere [13]. The Zn and Fe EXAFS spectra in a zinc-ferrite crystal were also measured so the performance of the EXAFS measuring system was verified and the parameters required for the EXAFS analysis were evaluated.

## 4. Results and discussion

Figure 2 shows the corrected coherent scattering intensity in electron units per atom as a function of the wavevector $|Q|$ for an amorphous zinc-ferrite film determined by ordinary x-ray scattering measurement with Mo Kα-radiation. The profile, consisting of the relatively sharp first peak and a few subsequent small peaks, is commonly observed in other oxide glasses [14]. This profile can easily be converted into the interference function $Qi(Q)$ and the RDF is then obtained by simply applying the Fourier transformation. However, it is readily imagined that determining the correlations of Zn–O and Fe–O pairs in zinc ferrite separately is difficult to achieve in x-ray diffraction, because both correlation distances in this glass are close to 0.2 nm. The use of the AXS method is now known to hold promise in that it would reduce this difficulty by allowing one to obtain the environmental RDFs around a specific element in multi-component non-crystalline systems.

Figure 3 gives two intensity profiles of an amorphous zinc-ferrite film measured at energies of 9.635 and 9.360 keV. Incidentally, these two energies are 25 and 300 eV below the Zn K-absorption edge (9.660 keV). Measurements at 7.086 and 6.811 keV

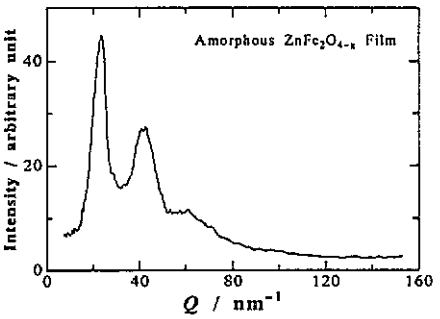


**Figure 2.** The scattering intensity profile obtained from an amorphous $ZnFe_2O_{4-x}$ film with Mo K$\alpha$-radiation.

below the Fe K-absorption edge (7.111 keV) were also carried out and the profiles are shown in figure 4. Theoretical values of the anomalous dispersion terms for Zn, Fe and O used in the present work and shown in figure 1 are found to agree well with the experimental ones at the lower energy side of the absorption edge [5]. The differential intensity profile for $Q$ less than 8 nm$^{-1}$ has been smoothly extrapolated to $Q = 0$. Such extrapolation is known to give no critical contribution in the calculation of the RDF by Fourier transformation [15].

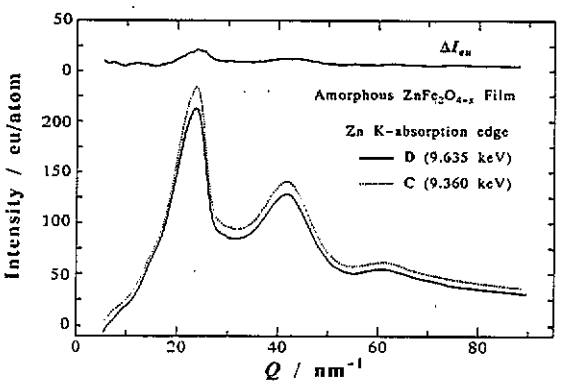


**Figure 3.** The differential intensity profile of an amorphous $ZnFe_2O_{4-x}$ film (top) obtained from the intensity profiles (bottom) measured at incident energies of 9.635 and 9.360 keV (D and C in figure 1), which correspond to energies of 25 and 300 eV below the Zn K-absorption edge.

Although the incident energies were selected at the lower energy side of the absorption edge, small amounts of fluorescent radiation were observed in the measurements at 9.635 and 7.086 keV, 25 eV below the edge. This arises mainly from the tail of the band pass of the monochromator crystal. In order to obtain sufficiently reliable structural information, such fluorescent components should be separated from the total intensity [5]. It is worth mentioning that the energy resolution of the Ge solid state detector is good enough to clearly separate the K$\alpha$ fluorescent radiations (8.630 keV for Zn and 6.399 keV for Fe) from the coherent scattering, whereas it is insufficient to separate the K$\beta$ fluorescent radiations (9.571 keV for Zn and 7.057 keV for Fe) from the coherent scattering. For this reason, the K$\beta$ fluorescent component overlapping the coherent scattering near the absorption edge was estimated from the

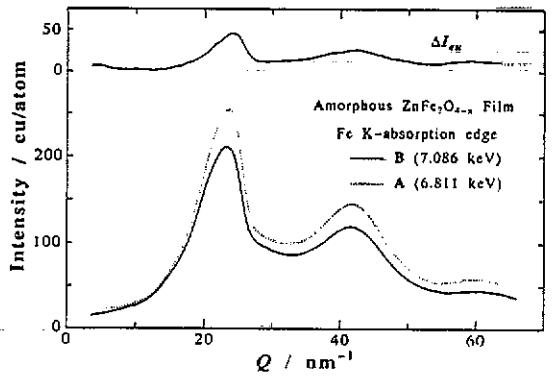


**Figure 4.** The differential intensity profile of an amorphous $ZnFe_2O_{4-x}$ film (top) obtained from the intensity profiles (bottom) measured at incident energies of 7.086 and 6.811 keV (B and A in figure 1), which correspond to energies of 25 and 300 eV below the Fe K-absorption edge.

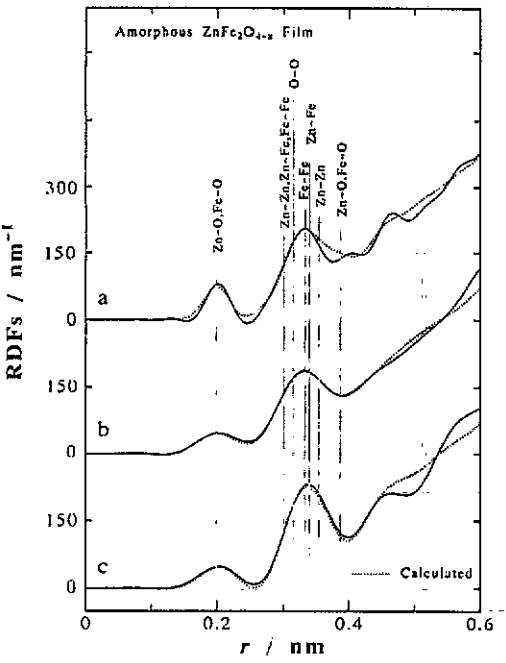


**Figure 5.** Experimental (solid) and calculated (dotted) ordinary radial distribution function (RDF) (curve a) and environmental RDFs for Zn (curve b) and Fe (curve c) in an amorphous $ZnFe_2O_{4-x}$ film. (Density = 4.7 Mg m$^{-3}$.)

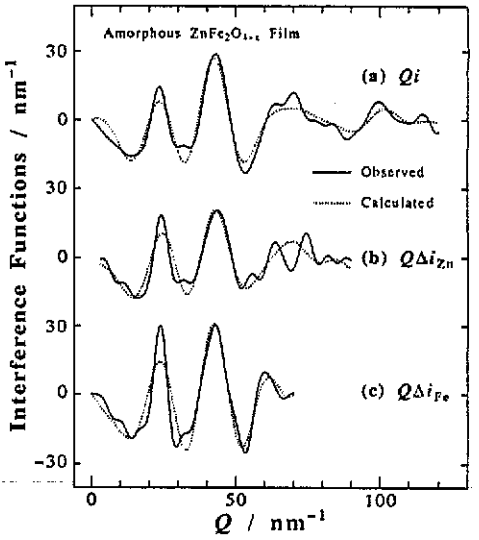


**Figure 6.** Experimental (solid) and calculated (dotted) ordinary interference function (curve a), and differential interference functions for Zn (curve b) and Fe (curve c) in an amorphous $ZnFe_2O_{4-x}$ film.

observed K$\alpha$ intensity and the tabulated K$\beta$ to K$\alpha$ ratio [16] and subtracted from the coherent scattering intensity. This method is now very common in AXS measurements.

Figure 5 shows the environmental RDFs for Zn and Fe in an amorphous zinc-ferrite film together with the ordinary RDF. Referring to the atomic distances between

nearest-neighbouring oxygen and transition metals in the crystalline zinc ferrite of normal spinel structure (0.200 and 0.206 nm), the first peaks of the environmental RDFs for Zn and Fe in figure 5 are ascribed to the Zn–O and Fe–O pairs, respectively. The oxygen coordination numbers around Zn or Fe estimated from these first peaks are 5.0 for Zn and 5.8 for Fe. Their experimental errors due to counting statistics [17] are ±0.5. These coordination numbers suggest that both Zn and Fe atoms are likely to occupy both tetrahedral and octahedral sites formed by oxygen ions. It should, however, be stressed that the reliability of the absolute values of these oxygen coordination numbers is not high enough to allow estimation of the details of a local ordering structure in this amorphous film. Both AXS data sets are restricted to the wavevector $|Q|$ range up to about 90 or 70 $nm^{-1}$, this arising from the relatively low energy absorption edges of Zn and Fe. This prevents us from obtaining the accurate environmental RDF due to the finite termination of the Fourier transformation and a careful interpretation is required [5]. The use of the least-squares technique, suggested by Levy *et al* [18], may be one way to reduce such inconvenience, using the interference functions instead of RDFs. This is particularly true in oxide glasses as characterized by a contrast between a distinct local ordering in the narrow region and a complete loss of the positional correlation at several nearest-neighbour distances away from the starting point.

According to Narten and Levy [19], the interference function may be given by the following expression.

$$Qi(Q) = \sum_{j=1}^{N}\sum_{k} x_j \frac{f_j f_k}{\langle f\rangle^2}\frac{N_{jk}}{r_{jk}}\exp(-b_{jk}Q^2)\sin Qr_{jk} + \sum_{\alpha=1}^{N}\sum_{\beta=1}^{N} x_\alpha x_\beta \frac{f_\alpha f_\beta}{\langle f\rangle^2} \times \exp(-b_{\alpha\beta}Q^2)4\pi\rho_0 \frac{QR_{\alpha\beta}\cos(QR_{\alpha\beta}) - \sin(QR_{\alpha\beta})}{Q^2} \tag{13}$$

where $N_{jk}$ is the average number of type-$k$ atoms around any type-$j$ atom at the average distance of $r_{jk}$ and the value of $b_{jk}$ is the mean square variation. The quantities of $R_{\alpha\beta}$ and $b_{\alpha\beta}$ correspond to the mean and the variance of the boundary region which need not be sharp [19, 20]. It is noted that the first and second terms on the RHS of (13) represent a discrete Gaussian-like distribution and a continuous distribution with an average number density in the longer distance, respectively. In practice, the distance and coordination number of interest in near-neighbour correlations are obtained by the least-squares calculation of (13) so as to reproduce the experimental interference function data. The differential interference function can be readily calculated by taking the difference between the ordinary interference function similarly estimated at the two energies in the AXS measurements and compared with the experimental data [21]. It is the intention of the authors that the structural parameters in the near-neighbour region should be more reasonably determined by applying this procedure so as to reproduce three independent experimental data of the AXS results for Zn and Fe and the ordinary result by Mo K$\alpha$-radiation, and the results are considered to be the best, at present, among several analytical procedures for the non-crystalline system.

Both tetrahedra and octahedra formed by oxygen may be feasible as the fundamental local ordering structures for providing discrete Gaussian-like distributions in the amorphous zinc-ferrite film. Then, as a first step, the starting parameters for the least-squares variations were set by slightly distorting the 14 near-neighbour correlations in a normal spinel crystal structure. However, the converged structural

parameters could not reproduce the AXS data for Zn. Thus, a similar trial calculation was made with the starting parameters calculated from different inversibility parameters $\alpha$, defined by $(1 - P_{Zn,t})/2$ where $P_{Zn,t}$ is the ratio of Zn atoms occupying the tetrahedral sites, i.e. $\alpha = 0$ for the normal spinel structure and $\alpha = 0.5$ for the inverse spinel structure. The starting parameters for $\alpha = 0.39$ gave the converged structural parameters which satisfy the three different RDFs in figure 5. The resultant parameters are listed in table 1 with the starting parameters. The errors of these parameters were estimated from the variance–covariance matrix in the non-linear least-squares variational method. The interference functions calculated from the resultant parameters in table 1 are compared with the observed ones in figure 6. The RDFs calculated by the Fourier transformation of these synthesized interference functions are described with dotted curves in figure 5.

**Table 1.** Summary of coordination numbers and distances in amorphous $ZnFe_2O_{4-x}$ film.

| | Spinel structure ($\alpha = 0.39$) | | Present study | | | |
|---|---|---|---|---|---|---|
| | | | AXS measurements | | EXAFS measurements | |
| Pairs | $r$ (nm) | $N$ | $r$ (nm) | $N$ | $r$ (nm) | $N$ |
| (tetrahedral site)–oxygen, (octahedral site)–oxygen | | | | | | |
| Zn–O | 0.203 | 5.6 | 0.202±0.002 | 5.4±0.5 | 0.201±0.002 | 4.6±0.7 |
| Fe–O | 0.201 | 5.2 | 0.198±0.002 | 5.7±0.4 | 0.196±0.002 | 5.4±0.7 |
| O–O | 0.298 | 12.0 | 0.311±0.005 | 11.6±1.8 | | |
| (octahedral site)–(octahedral site) | | | | | | |
| Zn–Zn | 0.298 | 1.8 | 0.295±0.004 | 1.8±0.3 | | |
| Zn–Fe | 0.298 | 2.9 | 0.310±0.002 | 2.6±0.2 | | |
| Fe–Fe | 0.298 | 2.3 | 0.295±0.003 | 1.8±0.2 | | |
| (tetrahedral site)–(octahedral site) | | | | | | |
| Zn–Zn | 0.349 | 2.1 | 0.351±0.004 | 1.0±0.3 | | |
| Zn–Fe | 0.349 | 5.3 | 0.338±0.002 | 2.0±0.2 | | |
| Fe–Fe | 0.349 | 5.7 | 0.341±0.002 | 3.7±0.2 | | |
| (tetrahedral site)–oxygen, (octahedral site)–oxygen | | | | | | |
| Zn–O | 0.360 | 8.9 | 0.371±0.003 | 7.7±0.7 | | |
| Fe–O | 0.357 | 9.6 | 0.353±0.002 | 8.7±0.4 | | |
| (tetrahedral site)–(tetrahedral site) | | | | | | |
| Zn–Zn | 0.364 | 0.2 | 0.369±0.077 | 0.2±0.3 | | |
| Zn–Fe | 0.364 | 0.7 | 0.360±0.010 | 0.6±0.2 | | |
| Fe–Fe | 0.364 | 1.2 | 0.370±0.006 | 0.9±0.2 | | |

The EXAFS spectra for Zn and Fe are shown in figure 7(a) and (b), respectively. By fitting the theoretical EXAFS spectrum in (11) to the experimental one in figure 7, the coordination numbers and atomic distances for the near-neighbour Zn–O and Fe–O pairs were determined and are also summarized in table 1. In both of the measurements, the atomic distance for the Zn–O pair is larger than that for the Fe–O pair which is the same tendency as observed in the original crystalline values. In spite of the near 10% or more experimental errors in the coordination numbers, it may be concluded that both Zn and Fe atoms occupy the positions of tetrahedral and octahedral sites formed by oxygen ions in the amorphous zinc-ferrite film. It may also be noted from figure 8 that the EXAFS RDFs of the amorphous zinc-ferrite film have only a single maximum, in contrast to the ones for the crystalline zinc ferrite.

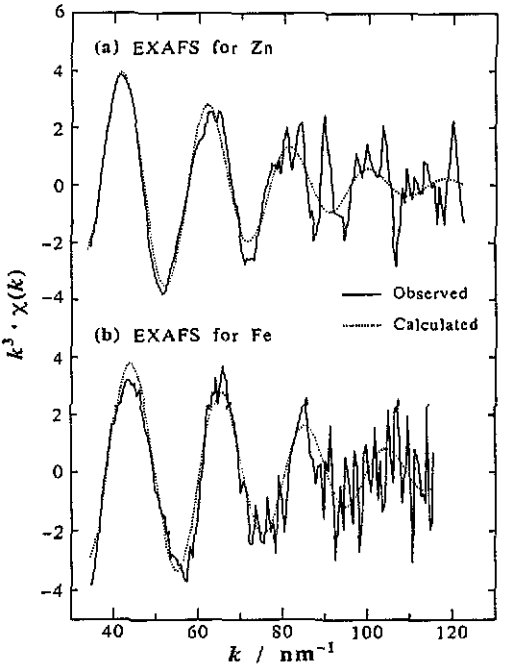


**Figure 7.** Experimental (solid) and calculated (dotted) EXAFS functions $k^3\chi(k)$ for (a) Zn and (b) Fe K-absorption edges. The parameters used for the calculations are $N = 5.4$ and $r = 0.200$ nm for Zn–O pairs, and $N = 5.2$ and $r = 0.196$ nm for Fe–O pairs.

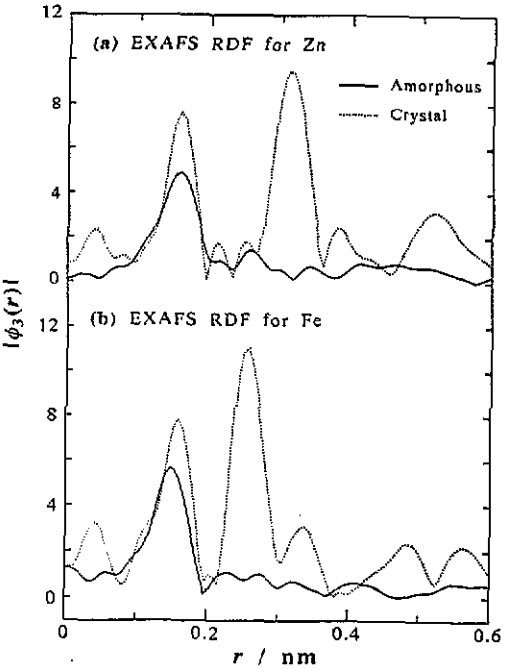


**Figure 8.** EXAFS radial distribution functions (RDFs) $|\phi_3(r)|$ for (a) Zn and (b) Fe in amorphous (solid) and crystalline (dotted) zinc ferrite.

The present authors also maintain the view, from the results presented here, that the least-squares method which was originally developed by Narten and his colleagues for the ordinary interference function becomes a more powerful tool for determining the near-neighbour correlations in multicomponent non-crystalline systems when in combination with the AXS measurements.

## Acknowledgments

The authors wish to thank Professor M Nomura, Photon Factory, National Laboratory for High-Energy Physics for his kind help on the AXS measurements (Proposal No 90-091). A part of this work was supported by the Grant-in-Aid for Scientific Research Fund from the Ministry of Education, Science and Culture of Japan (No 03 855 140 and 03 243 207).

## References

[1] Okuno S N, Hashimoto S, Inomata K, Morimoto S and Ito A 1990 *J. Mag. Soc. Japan* **14** 213
[2] Matsubara E, Waseda Y, Mitera M and Masumoto T 1988 *Trans. Japan Inst. Metals* **29** 697
[3] Weiner K L 1966 *Z. Kryst.* **123** 315

[4] Wagner C N J, Ocken H and Joshi M L 1965 *Z. Naturf.* a **20** 325
[5] Waseda Y 1984 *Novel Application of Anomalous X-ray Scattering for Structural Characterization of Disordered Materials* (Heidelberg: Springer) p 75
[6] Cromer D T and Liberman D 1970 *J. Chem. Phys.* **53** 1891
[7] James R W 1954 *The Optical Principles of the Diffraction of X-rays* (London: G Bell & Sons) p 135
[8] Teo B K 1986 *EXAFS Basic Principles and Data Analysis* (Heidelberg: Springer)
[9] Lee P A, Citrin P H, Eisenberger P and Kincaid B M 1981 *Rev. Mod. Phys.* **53** 61
[10] Matsubara E, Harada K, Waseda Y and Iwase M 1988 *Z. Naturf.* a **44** 723
[11] Ibers J A and Hamilton W C (ed) 1974 *International Tables for X-ray Crystallography* vol IV (Birmingham: Kynoch) pp 99, 149
[12] Cromer D T and Mann J B 1967 *J. Chem. Phys.* **47** 1892
[13] Oyanagi H, Ishigmo T, Tanoue H, Matsushita T and Kohza K 1984 *EXAFS and Near Edge Structure III (Springer Proceedings in Physics 2)* ed K O Hodgson, B Hedman and J E Penner-Hahn (Berlin: Springer) p 523
[14] Wright A C and Leadbetter A J 1976 *Phys. Chem. Glasses* **17** 122
[15] Furukawa K 1962 *Rep. Prog. Phys.* **25** 395
[16] Rao N V, Reddy S B, Satyanarayana G and Sastry D L 1986 *Physica* c **138** 215
[17] Matsubara E, Waseda Y, Ashizuka M and Ishida E 1988 *J. Non-Cryst. Solids* **103** 117
[18] Levy H A, Danford M D and Narten A H 1966 *ORNL Report No* ORNL-3960
[19] Narten A H and Levy H A 1969 *Science* **160** 447
[20] Narten A H 1972 *J. Chem. Phys.* **56** 1905
[21] Matsubara E, Sugiyama K, Waseda Y, Ashizuka M and Ishida E 1990 *J. Mater. Sci. Lett.* **9** 14